Synthesis of Delafossite $CuAlO_2$ p-Type Semiconductor using a Nanoparticle-Based Cu(I) Acetate-Loaded Boehmite Precursor

Tran V. Thu[a], Pham D. Thanh[a], Koichiro Suekuni[a], Nguyen H. Hai[b], Derrick Mott[a], Mikio Koyano[a], and Shinya Maenosono[a,*]

[a] *School of Materials Science, Japan Advanced Institute of Science and Technology (JAIST), 1-1 Asahidai, Nomi, Ishikawa 923-1292, Japan*

[b] *Center for Materials Science, College of Science, Vietnam National University (VNU), 334 Nguyen Trai, Hanoi, Vietnam*

*Corresponding author: Prof. S. Maenosono
E-mail: shinya@jaist.ac.jp
Tel: +81-761-51-1611
Fax: +81-761-51-1625

Abstract

Delafossite $CuAlO_2$ *p*-type nanostructured semiconductor was synthesized using boehmite (γ-AlOOH) nanorods loaded with copper(I) acetate [Cu(OAc)] as a precursor (nanoprecursor). Because Cu(OAc)-loaded γ-AlOOH nanorods are highly anisotropic, they tend to form inherent bunches consisting of several nanorods during the course of drying the nanoprecursor dispersion droplet on a solid substrate. By annealing the nanoprecursor at 1150 ºC in air, a delafossite $CuAlO_2$ polycrystal was successfully obtained as the dominant phase. The $CuAlO_2$ polycrystal is found to exhibit the (110) crystal orientation. The crystalline anisotropy of $CuAlO_2$, which is not usually attainable using conventional molecular precursors, is presumably originated in the anisotropic morphology of the nanoprecursor. The Seebeck coefficient, resistivity and thermal conductivity of the $CuAlO_2$ polycrystal at 300 K were found to be +560 $\mu V \cdot K^{-1}$, 1.3 Ω·m and 19.4 $W \cdot K^{-1} \cdot m^{-1}$, respectively, confirming the *p*-type nature of the $CuAlO_2$ polycrystal.

KEYWORDS: A. electronic materials, A. oxides, B. chemical synthesis, C. X-ray diffraction, D. crystal structure

1. Introduction

Transparent conducting oxides (TCOs) are very important for various kinds of devices and are commonly used in transparent electronics. The combination of low electrical resistivity and high transparency in the visible light range makes TCOs fascinating in various practical applications including liquid crystal displays, touch screens, photovoltaic devices, light emitting diodes, solar cells, etc [1-4]. Proverbially, most TCOs are *n*-type semiconductors. For example, Sn-doped In_2O_3 (ITO) [5], F-doped SnO_2 (FTO) [6] and Al-doped ZnO (AZO) [7] are all *n*-type materials. The lack of reliable preparation methods for *p*-type TCOs has prevented further developments of transparent electronics, which basically require *p*-*n* junctions. Cuprous aluminate delafossite ($CuAlO_2$) has been known as a *p*-type semiconductor since 1984 [8], and as a promising *p*-type TCO since its discovery by Hosono and coworkers in 1997 [9]. $CuAlO_2$ belongs to the family of delafossite TCOs [10,11]. This remarkable property is thought to be caused by its crystal structure, which is identified by alternating layers of dumbbell O-Cu-O and parallel planes of edge-shared octahedral AlO_6 (Fig. 1a) [9]. $CuAlO_2$ thin films have typically been prepared by high-vacuum physical vapour deposition techniques such as laser ablation [9,12], sputtering [13,14], and electron beam evaporation [15]. Meanwhile, some other techniques have also been employed to fabricate $CuAlO_2$ thin films, such as spray pyrolysis [16] and chemical vapour deposition [17,18]. If one can directly fabricate $CuAlO_2$ patterned thin films using wet processes, such as ink-jet printing, screen printing, spin coating, dip coating, spray coating, roll-to-roll coating, etc., the potential for dynamic development of transparent electronics drastically increases.

Toward this end, chemical synthetic routes of $CuAlO_2$ have been extensively investigated. For example, a powder containing the $CuAlO_2$ phase has been prepared from α-$LiAlO_2$ by ion exchange with CuCl at temperatures below 500 °C [19]. $CuAlO_2$ powders were also prepared using Cu_2O/CuO and Al_2O_3 powders in molten NaOH at 360 °C [20]. The polycrystalline $CuAlO_2$ was prepared by heating the stoichiometric mixture of high purity Al_2O_3

and Cu_2O at 1100 °C for four days in argon atmosphere, pelletizing it and reheating it at 1100 °C for two days [21]. $CuAlO_2$ thin films were prepared by thermal decomposition of a thin film composed of aluminum isopropoxide [$(CH_3)_2CHO_3Al$] and copper nitrate [$Cu(NO_3)_2{\cdot}5H_2O$] followed by crystallization at 1000-1100 °C [21]. $CuAlO_2$ thin films were also prepared by thermal decomposition of a thin film composed of copper acetate monohydrate [$Cu(OAc)_2{\cdot}H_2O$] and aluminum nitrate nonahydrate [$Al(NO_3)_3{\cdot}9H_2O$] followed by crystallization at 1000-1250 °C [22]. Moreover, a $CuAlO_2$ thin film was prepared by sol-gel processing using $Cu(OAc)_2{\cdot}H_2O$ and alumatrane [$Al(OCH_2CH_2)_3N$] as precursors and subsequent thermal treatment at 920 °C in air [23]. Interestingly, $CuAlO_2$ nanoparticles can be synthesized with $Cu(NO_3)_2{\cdot}3H_2O$ and $Al(NO_3)_3{\cdot}9H_2O$ precursors using the novel alkalotolerant and thermophilic fungus as a biocatalyst [24]. Among them, the most successful synthetic strategy may be the hydrothermal route [25-28]. Shannon and coworkers synthesized $CuAlO_2$ at relatively low temperature of 500-700 °C under high pressure [25-27]. $CuAlO_2$ was polycrystalline and could not be isolated as a pure phase. Shahriari *et al.* employed a Teflon pouch technique to synthesize $CuAlO_2$ from a mixture of CuO, Cu_2O, Al, and Al_2O_3. After a two-step thermal treatment (150 °C for 5 h and 210 °C for 48 h), the gray-black $CuAlO_2$ microcrystals were obtained [28]. Despite these efforts, it is still a big challenge to obtain pure phase *p*-type $CuAlO_2$ *via* a chemical synthetic route. The difficulty of synthesizing pure phase $CuAlO_2$ is mainly because it is a mixed oxide and Cu^+ tends to be easily oxidized to Cu^{2+}. To obtain pure phase $CuAlO_2$, an accurate control of reactant composition becomes essential. In addition, Cu^+ is unstable, and thus, is easily oxidized or reduced to metallic Cu^0 or Cu^{2+} depending on reaction conditions. Therefore, a strategy for the design of reaction is quite important to synthesize pure phase $CuAlO_2$ readily and reproducibly.

The nanocrystalline precursor (nanoprecursor) has a number of advantages over other molecular precursors. When one uses molecular precursors to fabricate $CuAlO_2$ thin films, the nucleation and grain growth would be left to nature even though they can be controlled to a

certain degree by varying annealing conditions. On the other hand, if one can mix bulk single crystals of cuprous oxide (Cu_2O) and γ-alumina (γ-Al_2O_3) together preserving crystallinity, it will be possible to obtain pure phase monocrystalline $CuAlO_2$. Obviously, however, such a process is quite challenging to realize. Nanoprecursors have the benefits of both molecular and bulk crystalline precursors. First, because nanoprecursors can be made in the forms of both powder and dispersion, they can be easily molded into the forms of bulk or thin film depending on applications. Second, a relatively uniform $CuAlO_2$ polycrystal in terms of composition and grain size can be obtained using nanoprecursors because of the nano-scale size and monodispersity. Third, if nanoprecursors have an anisotropic shape, i.e., one-dimensional nanorods, two-dimensional nanodiscs, etc., they can be spontaneously aligned to form an orientation-controlled higher-order structure during evaporation of solvent when one uses a nanoprecursor dispersion. Because anisotropic nanoparticles (NPs) are grown into a specific crystal direction as a result of preferential growth, if they align and sinter during calcination, the resulting $CuAlO_2$ polycrystal would have unidirectional grains. This is another interesting and important point of use of nanoprecursors.

In this study, we synthesized a pure phase $CuAlO_2$ polycrystal using monodispersed boehmite (γ-AlOOH) nanorods (NRs) and copper(I) acetate [Cu(OAc)] as precursors. γ-AlOOH NRs were synthesized by hydrolysis and dehydration of aluminum diacetate [$Al(OH)(OAc)_2$] *via* hydrothermal reaction. Then, γ-AlOOH NRs were mixed with Cu(OAc) in an appropriate solvent to form γ-AlOOH/Cu(OAc) composite NRs. By annealing the nanoprecursor at 1150 °C, a pure phase $CuAlO_2$ polycrystal was successfully synthesized. By pelletizing the nanoprecursor followed by annealing at 1150 °C, we obtained a gray-colored $CuAlO_2$ pellet and confirmed that it has *p*-type carriers.

2. Experimental

2.1. Materials

Aluminium acetate, basic [$Al(OH)(OAc)_2$] and copper(I) acetate [Cu(OAc)] were purchased from Sigma-Aldrich Corp., and solvents were purchased from Kanto Chemical Corp. All were used without further purification.

2.2. Synthesis of γ-AlOOH nanorods

In a typical synthesis, 3.5 mmol of $Al(OH)(OAc)_2$ was dissolved in 70 mL of distilled water, and then the resulting solution was transferred to an autoclave. The hydrothermal reaction was performed at 200 ºC for 12 hours. After which the autoclave was cooled down to room temperature, the reaction mixture was taken out, centrifuged and repeatedly washed several times with distilled water. The as-prepared product was dried in an oven at 60 ºC overnight to give white powders of γ-AlOOH (boehmite) NRs. The reaction yield was around 74%.

2.3. Preparation of γ-AlOOH/Cu(OAc) composite NRs (nanoprecursor)

γ-AlOOH (0.12 g, ca. 2 mmol) was mixed with Cu(OAc) (0.245 g, ca. 2 mmol) in 2 mL of pyridine. Pyridine was chosen because it is capable of dissolving both γ-AlOOH NRs and Cu(OAc) to form uniform dispersion. We call the dispersion as a nanoprecursor dispersion hereafter. The mixture was stirred for 6 hours under inert environment with the assistance of sonication. The mixture was then evaporated under low pressure (10^{-2} bar) to give a light green solid.

2.4. Thermal treatment of nanoprecursor

A light green solid was obtained by drying the nanoprecursor dispersion on a solid substrate. Then it was thermally treated for 2 hours at different temperatures (400, 600, 800, 1000, and 1150 ºC). Thermal treatment of samples in reducing atmosphere (Ar/H_2) resulted in metallic Cu (as confirmed from XRD). Therefore, all thermal treatments were conducted in air. For the measurements of the Seebeck coefficient, thermal conductivity, and electrical conductivity, the dried nanoprecursor was pelletized at 40 MPa followed by annealing at 1150 ºC for 4 hour. A gray pellet with 12 mm diameter was uni-axially pressed once again at 40 MPa and subsequently sintered at 1150 °C for 4 h in air in order to obtain a dense pellet.

2.5. Characterization

The samples were characterized by X-ray diffraction (XRD), transmission electron microscopy (TEM), selected-area electron diffraction (SAED), energy-dispersive X-ray spectroscopy (EDS), field-emission scanning electron microscopy (SEM), diffuse reflectance Fourier transform infrared spectroscopy (FT-IR), thermogravimetry (TG/DTG), and BET (Brunauer-Emmett-Teller) surface area analyzer. XRD data were obtained using a Rigaku RINT2500 diffractometer with Cu Kα radiation (λ = 1.542 Å; 40 kV, 100 mA). Morphology of samples was characterized using TEM and SEM. TEM samples were prepared by casting several microlitres of NR dispersion onto a carbon-coated Mo grid followed by drying in air. TEM images were obtained using Hitachi H-7100 and H-7650 transmission electron microscopes both operated at 100 kV. Elemental analyses were carried out using a Hitachi H-7650 transmission electron microscope equipped with an EDS detector. SAED patterns were recorded on an Hitachi H-9000NAR transmission electron microscope operated at 300 kV. SEM images were obtained using an Hitachi S4100 scanning electron microscope. FT-IR spectra were recorded on a Perkin Elmer Spectrum 100. TG/DTG data were obtained in air using a Seiko TG/DTA6200 (heating rate 10 °C·min^{-1}). The nitrogen adsorption and desorption isotherm of γ-AlOOH NRs were measured at 77K using a BELSORP-max surface area analyzer (BEL Japan, Inc.). Before the BET measurement, the samples were degassed and dehydrated in vacuum at 200 °C for 2 hours. The Seebeck coefficient, thermal conductivity, and electrical conductivity of the $CuAlO_2$ pellet were measured on a physical property measurement system (Quantum Design, PPMS) using the thermal transport option (TTO) package.

3. Results and discussion

3.1. Synthesis and characterization of γ-AlOOH NRs

Fig. 2a and b show high- and low-magnification TEM images of γ-AlOOH NRs, respectively. As seen in Fig. 2a and b, the NRs have a diameter of about ~10-30 nm and a length of about ~60-400 nm. The γ-AlOOH NRs are readily dispersed in water or other polar solvents

at high concentration with excellent colloidal stability. The inset of Fig. 2a shows a photograph of a NR dispersion taken 2 weeks after the preparation. No precipitation or aggregation was observed by visual inspection. Even after several months, there was no significant change in the appearance. The excellent stability of NRs occurs presumably because the surfaces of NRs are well hydrated. Fig. 2c shows an SEM image of γ-AlOOH NRs. They tend to form inherent bunches consisting of several NRs. The alignment of these highly anisotropic NRs is presumably achieved during the course of drying the nanoprecursor dispersion droplet on a solid substrate. Fig. 2d shows the XRD pattern of γ-AlOOH NRs indicating that the NRs have an orthorhombic γ-AlOOH single phase (Fig. 1b). The primary peak in the XRD pattern corresponds the (200) plane as indicated by the γ-AlOOH reference pattern. This indicates that the γ-AlOOH NRs grew along the *a*-axis. This structural feature did not change even when the reaction conditions were varied. In general, chemically synthesized γ-AlOOH NPs tend to have one-dimensional morphologies, e.g. nanowires [29], nanofibers [30,31] and nanorods [32-42], which is similar to our result. The chemical equations of the reaction can be expressed as:

$$Al(OH)(OAc)_2 + 2H_2O \rightarrow Al(OH)_3 + 2CH_3COOH \quad (1)$$

$$Al(OH)_3 \rightarrow AlOOH + H_2O \quad (2)$$

Dehydration reaction [Equation (2)] might be initiated with increase in temperature or decrease in pH [43,44]. The as-produced CH_3COOH might act as a shape directing agent adsorbing onto specific crystalline planes of γ-AlOOH to promote preferential growth of γ-AlOOH, and thus, γ-AlOOH NRs were selectively formed. Finally, the surface area of γ-AlOOH NRs was determined by the BET (Brunauer-Emmett-Teller) surface area analyzer. As a result, the specific BET surface area was estimated to be 38 $m^2 \cdot g^{-1}$. If one assumes that a γ-AlOOH NR has

a cylindrical shape with diameter of 30 nm and length of 400 nm, the theoretical value is calculated to be 45.7 $m^2 \cdot g^{-1}$, which is comparable to the BET surface area. This result suggests that the surfaces of γ-AlOOH NRs are smooth without mesopores.

3.2. Phase transformation behaviour of γ-AlOOH NRs

Because γ-AlOOH NRs will be used as a precursor and be calcined together with copper precursor to form $CuAlO_2$ in the next step, the thermal behaviour of γ-AlOOH NRs was analyzed by thermogravimetry (TG/DTG). Fig. 3 shows a TG/DTG result with respect to the γ-AlOOH NRs. The slight mass loss observed below 200 ºC (~ 4%) is attributed to desorption of physisorbed water. The mass loss observed between 300 ºC and 500 ºC is assigned to the phase transformation from γ-AlOOH to Al_2O_3. The observed amount of the mass loss was ~ 16% which agrees well to the theoretical mass loss of 15% calculated according to Equation (3).

$$2AlOOH \rightarrow Al_2O_3 + H_2O \quad (3)$$

In order to examine this further, we carried out structural characterizations for the sample obtained by thermal treatment of γ-AlOOH NRs at 600 ºC for 1 hour in air. After the thermal treatment, a white solid material was obtained. Fig. 4a and b show high- and low-magnification TEM images of the product, respectively. As seen in Fig. 4a and b, the NRs have a diameter of about ~10-20 nm and a length of about ~40-300 nm. Comparing these dimensions with those of γ-AlOOH NRs, the NRs have almost the same diameter as γ-AlOOH NRs, but have a shorter length than γ-AlOOH NRs. Fig. 4c shows the SAED pattern of the NRs, which corresponds to the γ-Al_2O_3 phase. The XRD pattern of the NRs (Fig. 4d) agrees well with cubic γ-Al_2O_3. The thermal decomposition of γ-AlOOH starts with the removal of the structural water molecules followed by the crystallization of γ-Al_2O_3. The primary peak in the XRD pattern corresponds the (400) plane as indicated by the γ-Al_2O_3 reference pattern. These results clearly indicate that the

phase transformation from γ-AlOOH NRs to γ-Al_2O_3 NRs was completed without a significant architectural change, which is consistent with previous reports [45,46]. Surprisingly, the γ-Al_2O_3 NRs are still readily-dispersible in water or other polar solvents at high concentration with excellent colloidal stability.

To further confirm the phase transformation from γ-AlOOH to γ-Al_2O_3, and to inspect the purity, we conducted FT-IR measurements for γ-AlOOH and γ-Al_2O_3 NRs. Fig. 5 shows the FT-IR spectra of both NRs. In the case of γ-AlOOH NRs, the intense bands at 3300 and 3112 cm^{-1} correspond to asymmetric ν_{as}(Al)O-H and symmetric ν_s(Al)O-H stretching vibrations, respectively. These two strong and well-separated bands are indicative of a good crystallinity of γ-AlOOH NRs [38]. The peaks at 1556 and 1651 cm^{-1} represent bending modes of adsorbed water. Two peaks at 1147 and 1062 cm^{-1} are ascribed to asymmetric δ_{as}Al-O-H and symmetric δ_sAl-O-H bending vibration in the crystal lattice. The broad peak at 620 cm^{-1} corresponds to the vibration mode of AlO_6 octahedra. In the case of γ-Al_2O_3 NRs, two peaks at 3468 cm^{-1} (broad) and 1647 cm^{-1} (sharp) are observed corresponding to stretching vibrations of -OH group on the surface of γ-Al_2O_3 NRs and bending mode of adsorbed water, respectively. The broad peak at 576 cm^{-1} corresponds to the vibration mode of AlO_6 octahedra. In consequence, it is verified that the as-synthesized γ-AlOOH NRs and γ-Al_2O_3 NRs are pure phase without impurities.

3.3. Preparation and characterization of γ-AlOOH/Cu(OAc) composite nanoprecursor

To prepare the nanoprecursor for the $CuAlO_2$ synthesis, γ-AlOOH NRs and Cu(OAc) were simultaneously dissolved in pyridine at a Cu/Al atomic ratio of 1:1 (Scheme 1). TEM and SEM images of the sample (Fig. 6a and b) confirmed that Cu(OAc) were homogeneously deposited onto all the surfaces of the γ-AlOOH NRs. Fig. 6c shows a photograph of the nanoprecursor dispersion. The well-dispersed stable dispersion is a promising material for wet processing. If one takes a close look at Fig. 6a and b, Cu(OAc) is found to be homogeneously attached on the NR surfaces. The homogeneous attachment of Cu(OAc) on γ-AlOOH NRs is

thought to be a good sign for the synthesis of uniform $CuAlO_2$ polycrystal. In addition, the hydrophobic interaction [47] between Cu(OAc) may facilitate a self-assembly of NRs. This structure is quite beneficial for the subsequent solid state reaction because of the huge number density of reactive spots, where the reaction takes place, and the quite-short diffusion length thanks to the nano-scale dimension.

To further confirm the formation of γ-AlOOH/Cu(OAc) nanocomposite, the elemental composition of a small area containing just a few NRs was analyzed using TEM-EDS. Fig. 6d shows the TEM-EDS spectrum confirming the presence of Cu (26.6 atom%), Al (26.5 atom%) and O (46.9 atom%) in the nanocomposite evidencing the homogeneous distribution of Cu(OAc) in the NR framework. Note that Mo and C peaks seen in the EDS spectrum are from the carbon-coated Mo grid.

3.4. Phase transformation behaviour of γ-AlOOH/Cu(OAc) composite nanoprecursor

Fig. 7 shows TEM and SEM images of γ-AlOOH/Cu(OAc) nanocomposite annealed for 2 h at different temperatures: 400, 600, 1000, and 1150 ºC. As seen in Fig. 7a, the morphology of NRs did not change much after annealing at 400 ºC. However, small NPs (black spots in the TEM image) seem to have aggregated. Fig. 8a shows an XRD pattern of γ-AlOOH/Cu(OAc) nanocomposite annealed at 400 ºC. The XRD pattern clearly shows coexistence of γ-AlOOH and CuO phases. This indicates that Cu(OAc) is oxidized to form CuO according to the following reaction:

$$4Cu(OAc) + 9O_2 \rightarrow 4CuO + 8CO_2 + 6H_2O \qquad (4)$$

On the other hand, the phase transformation from γ-AlOOH to γ-Al_2O_3 had not proceeded much, and thus, no γ-Al_2O_3 was observed.

When the annealing temperature was increased to 600 ºC, NPs become sintered to form larger NPs as shown in Fig. 7b. However, the morphology of the NRs remains unchanged. Fig.

8b shows an XRD pattern of γ-AlOOH/Cu(OAc) nanocomposite annealed at 600 ºC. The XRD pattern shows the disappearance of the γ-AlOOH phase and a coexistence of γ-Al_2O_3 and CuO phases. This result is reasonable because the phase transformation from γ-AlOOH to γ-Al_2O_3 was found to be completed when it was annealed at 600 ºC for 1 hour in air (see Fig. 4).

When the γ-AlOOH/Cu(OAc) nanocomposite was annealed at 1000 ºC, both NRs and NPs become sintered together to form bigger crystals as shown in Fig. 7c. Fig. 8d shows an XRD pattern of the sample. It is evidenced that CuO and copper aluminate spinel ($CuAl_2O_4$) phases dominantly coexist. This phase transformation reaction can be expressed as

$$CuO + Al_2O_3 \rightarrow CuAl_2O_4 \qquad (5)$$

At this temperature, the reaction between CuO NPs and γ-Al_2O_3 NRs eventually takes place. To determine the threshold temperature for the solid state reaction between CuO and γ-Al_2O_3, we annealed the γ-AlOOH/Cu(OAc) nanocomposite at 800 ºC. Fig. 8c shows an XRD pattern of the sample annealed at 800 ºC. In this case, the coexistence of CuO and $CuAl_2O_4$ phases is also observed, while the relative intensity of peaks corresponding to $CuAl_2O_4$ phase is much lower than those of Fig. 8d. This means that the threshold temperature for the solid state reaction between CuO and γ-Al_2O_3 might be in between 600 and 800 ºC.

Finally the annealing temperature was further increased up to 1150 ºC. As shown in Fig. 7d, all nanoparticulate morphologies disappeared and large crystals emerged. However, the large crystal still retains some remnants of NR morphology in its internal structure. Fig. 8e shows an XRD pattern of the sample annealed at 1150 ºC. In this case, $CuAlO_2$ is the dominant phase with some very minor peaks corresponding to the $CuAl_2O_4$ phase. Reflecting the large grain size, the XRD peaks are much sharper than those of samples annealed at lower temperatures. This phase transformation reaction can be expressed as

$$2CuO + 2CuAl_2O_4 \rightarrow 4CuAlO_2 + O_2 \quad (6)$$

We also found that, if the Cu/Al atomic ratio was less than 1, the relative intensity of $CuAl_2O_4$ peaks increased at this temperature. When the Cu/Al atomic ratio was 0.5, the dominant phase was switched to $CuAl_2O_4$. The average grain size of $CuAl_2O_4$ phase estimated by the Scherrer formula using the (311) primary peak also dramatically increased with decreasing the Cu/Al atomic ratio. This phenomenon can be elucidated by two different mechanisms. First, CuO phase is consumed faster than Al_2O_3 phase according to Equation (5) preventing the reaction expressed by Equation (6), because of the Al-rich composition. Second, $CuAlO_2$ phase once formed might return to $CuAl_2O_4$ phase according to Equation (7).

$$4CuAlO_2 + 2Al_2O_3 + O_2 \rightarrow 4CuAl_2O_4 \quad (7)$$

As seen in Fig. 8e, the relative (110) peak intensity of the $CuAlO_2$ polycrystal synthesized using a nanoprecursor followed by annealing at 1150 ºC is significantly enhanced compared to the standard pattern for $CuAlO_2$ bulk crystal. This result indicates that our $CuAlO_2$ polycrystal has an orientation along the (110) lattice planes. The crystal structure of $CuAlO_2$ can be described as the alternate stacking of edge shared AlO_6 octahedral layers and Cu^+ ion layers perpendicular to the *c*-axis. Each of the Cu^+ ion layers is linearly coordinated by two O^{2-} anions. The energy levels of Cu^+ and O 2p overlap, giving rise to increased mobility of holes, which makes them suitable for *p*-type conduction. Because of this structural anisotropy, electrical conductivity along the *ab* plane was reported to be over 25-fold higher than that along the *c* axis [48], indicating that the main conduction path of the $CuAlO_2$ polycrystal is closed-packed Cu^+ layers (see Fig. 1a). For this reason, the (110)-oriented $CuAlO_2$ polycrystal synthesized in the present study is quite promising, because such a structure is usually unattainable using solid state chemical synthesis.

3.5. Assessment of the electrical/thermal properties of $CuAlO_2$ synthesized using γ-AlOOH/Cu(OAc) nanoprecursor

For the measurements of the Seebeck coefficient, thermal conductivity, and electrical conductivity, the dried nanoprecursor was pelletized at 40 MPa followed by annealing at 1150 ºC for 4 hours. A gray pellet of 12 mm diameter was uni-axially pressed once again at 40 MPa and subsequently sintered at 1150 °C for 4 h in air in order to obtain a dense pellet. Fig. 9 shows a photograph of a piece of the pellet (mass of 33.04 mg, area of 3.6×3.4 mm^2 and thickness of 0.6 mm). The density of the pellet was 4.4 g·cm^{-3}, 87% of the theoretical value. Then, two side surfaces of the pellet were coated with gold paste to contact with the electrodes of the sample holder. As seen in Fig. 9, the color of the $CuAlO_2$ pellet is blue-gray or gray-black. Similar results have been reported in the literature. For example, the colour of $CuAlO_2$ fibrous mats appeared to be gray [49], whereas $CuAlO_2$ samples synthesized by solid state reaction hydrothermal processing were correspondingly blue-gray and gray-black [50]. In the case of $CuAlO_2$ synthesized *via* ion exchange [19], a large amount of deep states in the forbidden band gap of $CuAlO_2$ were thought to be the reason for the blue-gray colour. Our observation agrees well with the previous reports. Interestingly, as seen in Fig. 8f, the relative (110) peak intensity of the $CuAlO_2$ pellet dramatically decreased compared to that of $CuAlO_2$ polycrystal before pelletizing (Fig. 8e), and the relative intensities of all peaks are almost identical to the standard pattern for $CuAlO_2$ bulk crystal. This result suggests that the (110) crystal orientation was destroyed during pelletizing. Note that the weak peaks observed at 31.3, 36.0, 38.8, 59.6 and 66.3 degrees in Fig. 8f correspond to $CuAl_2O_4$(220), CuO($\bar{1}$11)/(002), CuO(111)/(200), $CuAl_2O_4$(511) and CuO (022)/ ($\bar{3}$11), respectively.

The Seebeck coefficient (S), resistivity (ρ), and thermal conductivity (κ) of the $CuAlO_2$ pellet were measured using a physical property measurement system (Quantum Design, PPMS) using the thermal transport option (TTO) package with two electrodes. As a result, the values of

S, ρ, and κ at 300 K are found to be 560 $\mu V \cdot K^{-1}$, 1.3 $\Omega \cdot m$, and 19.4 $W \cdot K^{-1} \cdot m^{-1}$, respectively. The sign of *S* is positive confirming *p*-type conductivity. The magnitude of the Seebeck coefficient is fairly large (indicative of semiconducting behaviour) compared to that of a $CuAlO_2$ single crystal (~300 $\mu V \cdot K^{-1}$ at 300 K) [51]. On the other hand, the resistivity is an order of magnitude larger than that of single crystal (~0.15 $\Omega \cdot m$ at 300 K) [51]. The thermal conductivity, κ, of $CuAlO_2$ is reported to be strongly depending on grain size. For example, in the case of bulk crystal, κ is ~20 $W \cdot K^{-1} \cdot m^{-1}$ at 300 K, while it decreases to ~2 $W \cdot K^{-1} \cdot m^{-1}$ at 300 K in the cases of nanocrystalline $CuAlO_2$ and disordered $CuAlO_2$ crystal [52]. This means that our pellet sample has almost the same thermal conductivity as bulk $CuAlO_2$ crystal.

4. Conclusions

Delafossite $CuAlO_2$ was synthesized using γ-AlOOH NRs loaded with Cu(OAc) as a precursor. The γ-AlOOH NRs were synthesized by a facile hydrothermal technique and the resulting NRs were found to grow along the *a*-axis. The NRs were monodispersed and readily dispersible in water at high concentration. By mixing the NRs with Cu(OAc) in pyridine, γ-AlOOH/Cu(OAc) composite NRs (nanoprecursor) were obtained. Cu(OAc) was homogeneously loaded onto all the NR surfaces. The nanoprecursor was then annealed at different temperatures. As a result, the phase transformation of the nanoprecursor was found to go through the following path: (1) Cu(OAc) become CuO NPs while γ-AlOOH NRs remain unchanged at $T \leq$ 400 ºC, where *T* denotes the annealing temperature. (2) When T = 600 ºC, γ-AlOOH NRs start to be transformed into γ-Al_2O_3 NRs. Simultaneously, CuO NPs react with γ-Al_2O_3 NRs to form copper aluminate spinel ($CuAl_2O_4$) phase. (3) When *T* is elevated further to 1000 ºC, the fraction of $CuAl_2O_4$ phase increases as a result of reaction between CuO and γ-Al_2O_3 phases. (4) When T = 1150 ºC, delafossite $CuAlO_2$ phase appears as the dominant phase. Interestingly, the $CuAlO_2$ polycrystal exhibits the (110) orientation presumably due to the crystalline anisotropy of the nanoprecursor. The Seebeck measurement for the $CuAlO_2$ polycrystal confirmed that at room

temperature the primary charge carriers are holes with a relatively large Seebeck coefficient of 560 $\mu V \cdot K^{-1}$.

Acknowledgements

Tran V. Thu acknowledges the Vietnamese government for a 322 scholarship and financial support from the Cooperation Independent Research Foundation (JAIST). The authors wish to thank Prof. Tatsuya Shimoda and Kazuhiro Fukada for their generous support for the TG/DTA measurements.

References

_[1] B. G. Lewis, D. C. Paine, MRS Bull. (2000) 22.

_[2] Y. Yang, L. Wang, H. Yan, S. Jin, T. J. Marks, S. Y. Li, Appl. Phys. Lett. 89 (2006) 051116.

_[3] M. Emziane, K. Durose, D. P. Halliday, A. Bosio, N. Romeo, Appl. Phys. Lett. 87 (2005) 251913.

_[4] D. Ginley, T. Coutts, J. Perkins, D. Young, X. Li, P. Parilla, MRS Proc. (2001) 668.

_[5] C. G. Granqvist, A. Hultaker, Thin Solid Films 411 (2002) 1.

_[6] K. L. Chopra, S. Major, D. K. Pandya, Thin Solid Films 102 (1983) 1.

_[7] T. V. Thu, S. Maenosono, J. Appl. Phys. 107 (2010) 014308.

_[8] F. A. Benko, F. P. Koffyberg, J. Phys. Chem. Solids 45 (1984) 57.

_[9] H. Kawazoe, M. Yasukawa, H. Hyodo, M. Kurita, H. Yanagi, H. Hosono, Nature 389 (1997) 939.

[10] R. D. Shannon, Acta Cryst. A 32 (1976) 751.

[11] T. Ishiguro, N. Ishizawa, N. Mizutani, M. Kato, Acta Cryst. B 39 (1983) 564.

[12] H. Yanagi, S. Inoue, K. Ueda, H. Kawazoe, H. Hosono, N. Hamada, J. Appl. Phys. 88 (2000) 4159.

[13] N. Tsuboi, T. Moriya, S. Kobayashi, H. Shimizu, K. Kato, F. Kaneko, Jpn. J. Appl. Phys. 47 (2008) 592.

[14] A. N. Banerjee, K. K. Chattopadhyay, J. Appl. Phys. 97 (2005) 084308.

[15] D. S. Kim, S. J. Park, E. K. Jeong, H. K. Lee, S. Y. Choi, Thin Solid Films 515 (2007) 5103.

[16] C. Bouzidi, H. Bouzouita, A. Timoumi, B. Rezig, Mater. Sci. Eng. B 118 (2006) 259.

[17] H. Gong, Y. Wang, Y. Luo, Appl. Phys. Lett. 76 (2000) 3959.

[18] Y. Wang, H. Gong, Chem. Vap. Deposition 6 (2000) 285.

[19] L. Dloczik, Y. Tomm, R. Konenkamp, M. C. Lux-Steiner, Th. Dittrich, Thin Solid Films 451-452 (2004) 116.

[20] B. Saha, R. Thapa, K. K. Chattopadhyay, Mater. Lett. 63 (2009) 394.

[21] X. G. Zheng, K. Taniguchi, A. Takahashi, Y. Liu, C. N. Xu, Appl. Phys. Lett. 85 (2004) 1728.

[22] G. Li, X. Zhu, H. Lei, H. Jiang, W. Song, Z. Yang, J. Dai, Y. Sun, X. Pan, S. Dai, J. Sol-Gel Sci. Technol. 53 (2010) 641.

[23] S. Gotzendorfer, C. Polenzky, S. Ulrich, P. Lobmann, Thin Solid Films 518 (2009) 1153.

[24] A. Ahmad, T. Jagadale, V. Dhas, S. Khan, S. Patil, R. Pasricha, V. Ravi, S. Ogale, Adv. Mater. 19 (2007) 3295.

[25] R. D. Shannon, D. B. Rogers, C. T. Prewitt, Inorg. Chem. 10 (1971) 713.

[26] C. T. Prewitt, R. D. Shannon, D. B. Rogers, Inorg. Chem. 10 (1971) 719.

[27] D. B. Rogers, R. D. Shannon, C. T. Prewitt, J. L. Gillson, Inorg. Chem. 10 (1971) 723.

[28] D. Y. Shahriari, A. Barnabè, T. O. Mason, K. R. Poeppelmeier, Inorg. Chem. 40 (2001) 5734.

[29] J. Zhang, S. Wei, J. Lin, J. Luo, S. Liu, H. Song, E. Elawad, X. Ding, J. Gao, S. Qi, C. Tang, J. Phys. Chem. B 110 (2006) 21680.

[30] S. C. Kuiry, E. Megen, S. D. Patil, S. A. Deshpande, S. Seal, J. Phys. Chem. B 109 (2005) 3868.

[31] Y. Mathieu, B. Lebeau, V. Valtchev, Langmuir 23 (2007) 9435.

[32] H. C. Lee, H. J. Kim, S. H. Chung, K. H. Lee, H. C. Lee, J. S. Lee, J. Am. Chem. Soc. 125 (2003) 2882.

[33] J. Zhang, S. Liu, J. Lin, H. Song, J. Luo, E. M. Elssfah, E. Ammar, Y. Huang, X. Ding, J. Gao, S. Qi, C. Tang, J. Phys. Chem. B 110 (2006) 14249.

[34] Y. Zhao, R. L. Frost, W. N. Martens, H. Y. Zhu, Langmuir 23 (2007) 9850.

[35] T. He, L. Xiang, S. Zhu, CrystEngComm 11 (2009) 1338.

[36] J. Zhang, F. Shi, J. Lin, S. Y. Wei, D. Chen, J. M. Gao, Z. Huang, X. X. Ding, C. Tang, Mater. Res. Bull. 43 (2008) 1709.

[37] M. G. Ma, Y. J. Zhu, Z. L. Xu, Mater. Lett. 67 (2007) 1812.

[38] T. He, L. Xiang, S. Zhu, Langmuir 24 (2008) 8284.

[39] X. Y. Chen, Z. J. Zhang, X. L. Li, S. W. Lee, Solid State Commun. 145 (2008) 368.

[40] T. S. Chang, J. H. Na, C. Y. Jung, S. M. Koo, J. Ceram. Process Res. 10 (2009) 832.

[41] Y. Deng, Q. Yang, G. Lu, W. Hu, Ceram. Inter. 36 (2010) 1773.

[42] S. C. Shen, Q. Chen, P. S. Chow, G. H. Tan, X. T. Zeng, Z. Wang, R. B. H. Tan, J. Phys. Chem. C 111 (2007) 700.

[43] T. Tamura, M. L. Jackson, Science 117 (1953) 381.

[44] W. O. Milligan, J. Phys. Chem. 55 (1951) 497.

[45] S. J. Wilson, J. Solid State Chem. 30 (1979) 247.

[46] G. Paglia, E. S. Božin, S. J. L. Billinge, Chem. Mater. 18 (2006) 3242.

[47] D. Chandler, Nature 437 (2005) 640.

[48] M. S. Lee, T. Y. Kim, D. Kim, Appl. Phys. Lett. 79 (2001) 2028.

[49] S. Zhao, M. Li, X. Liu, G. Han, Mater. Chem. Phys. 116 (2009) 615.

[50] D. Y. Shahriari, A. Barnabe, D. Ko, K. R. Poeppelmeier, Chem. Mater. 16 (2004) 5616.

[51] J. Tate, H. L. Ju, J. C. Moon, A. Zakutayev, A. P. Richard, J. Russell, D. H. McIntyre, Phys. Rev. B 80 (2009) 165206.

[52] O. J. Durá, R. Boada, A. Rivera-Calzada, C. León, E. Bauer, M. A. López de la Torre, J. Chaboy, Phys. Rev. B 83 (2011) 045202.

Scheme caption

Scheme 1. From preparation of γ-AlOOH/Cu(OAc) composite nanoprecursor to the synthesis of $CuAlO_2$ polycrystal.

Figure captions

Fig. 1. Crystal structures of (a) delafossite $CuAlO_2$ and (b) boehmite (γ-AlOOH). Red, blue and pink spheres represent O, Cu and Al atoms, respectively.

Fig. 2. High- (a) and low-magnification (b) TEM, and (c) SEM images of γ-AlOOH NRs. The inset of panel a shows a photograph of an aqueous dispersion of γ-AlOOH NRs taken 2 weeks after the preparation. (d) XRD pattern of γ-AlOOH NRs. Bars indicate reference peaks of γ-AlOOH (JCPDS card no. 01-072-0359).

Fig. 3. TG and DTG curves of γ-AlOOH NRs.

Fig. 4. High- (a) and low-magnification (b) TEM images, and (c) SAED pattern of γ-Al_2O_3 NRs. (d) XRD pattern of γ-Al_2O_3 NRs. Bars indicate reference peaks of γ-Al_2O_3 (JCPDS card no. 01-079-1558).

Fig. 5. Diffuse reflectance IR spectra of γ-AlOOH (bottom) and γ-Al_2O_3 NRs (top).

Fig. 6. (a) TEM and (b) SEM images of γ-AlOOH/Cu(OAc) composite nanoprecursor. (c) A photograph of a pyridine dispersion of the nanoprecursor. (d) TEM-EDS spectrum of γ-AlOOH/Cu(OAc) composite nanoprecursor.

Fig. 7. TEM (left) and SEM (right) images of samples after annealing at (a) 400, (b) 600, (c) 1000, and (d) 1150 ºC.

Fig. 8. XRD patterns of samples after annealing at (a) 400, (b) 600, (c) 800, (d) 1000, and (e) 1150 ºC. The indexed peaks are marked by the symbols open triangle (△) for γ-AlOOH (JCPDS card no. 01-072-0359), filled squares (■) for CuO (JCPDS card no. 01-070-6827), open circles (○) for $CuAl_2O_4$ (JCPDS card no. 01-071-0966), and open diamond (◇) for γ-Al_2O_3 (JCPDS card no. 01-079-1558). (f) XRD pattern of the $CuAlO_2$ pellet. Bars indicate reference peaks of $CuAlO_2$ (JCPDS card no. 01-075-2359).

Fig. 9. Photograph of the $CuAlO_2$ pellet (mass of 33.04 mg, area of 3.6×3.4 mm^2 and thickness of 0.6 mm) used for the PPMS-TTO measurement.

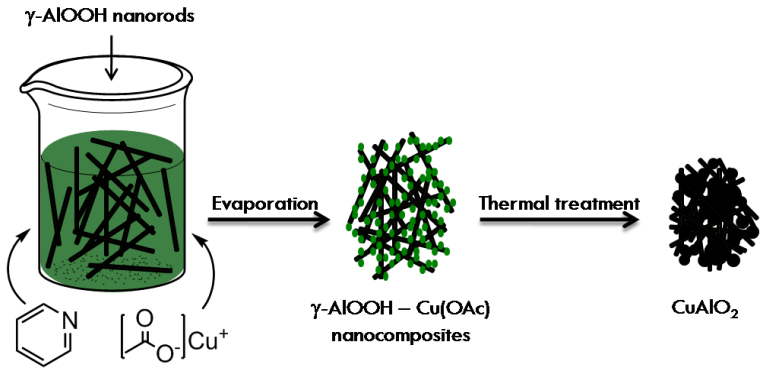

Scheme 1

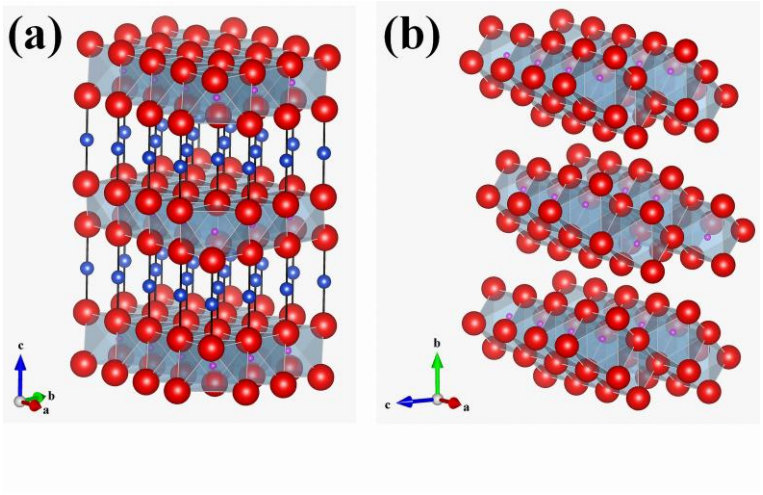

Fig. 1

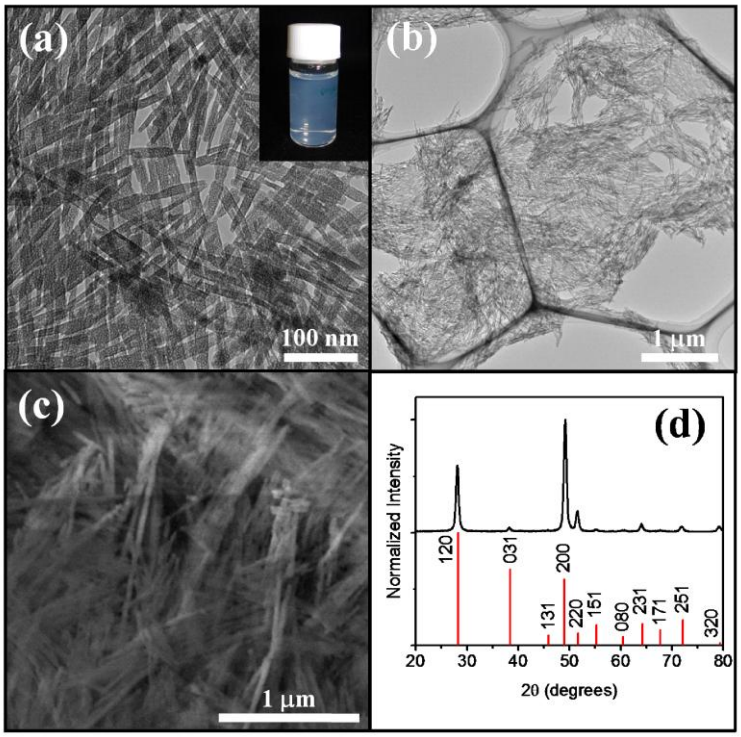
(a)
100 nm
(b)
1 μm
(c)
1 μm
(d)
Normalized Intensity
120
031
200
131
220
151
080
231
171
251
320
20
30
40
50
60
70
80
2θ (degrees)

Fig. 2

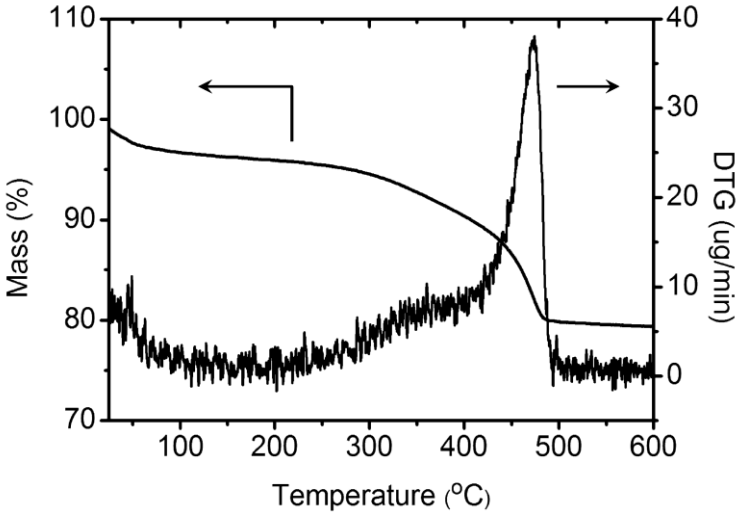
110
100
90
80
70
Mass (%)
40
30
20
10
0
DTG (ug/min)
100
200
300
400
500
600
Temperature (°C)

Fig. 3

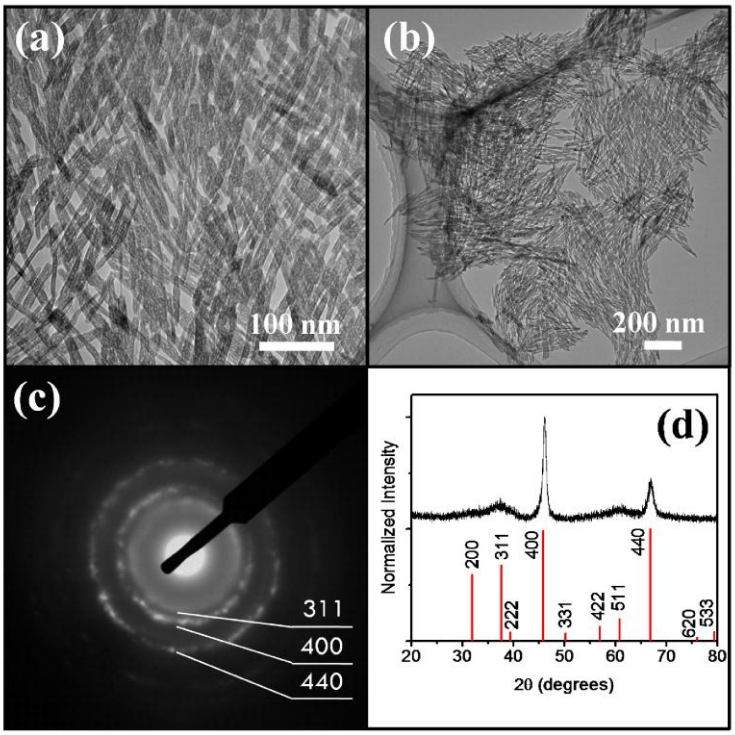
(a)
100 nm
(b)
200 nm
(c)
311
400
440
(d)
Normalized Intensity
200
311
400
222
331
422
511
440
620
533
20
30
40
50
60
70
80
2θ (degrees)

Fig. 4

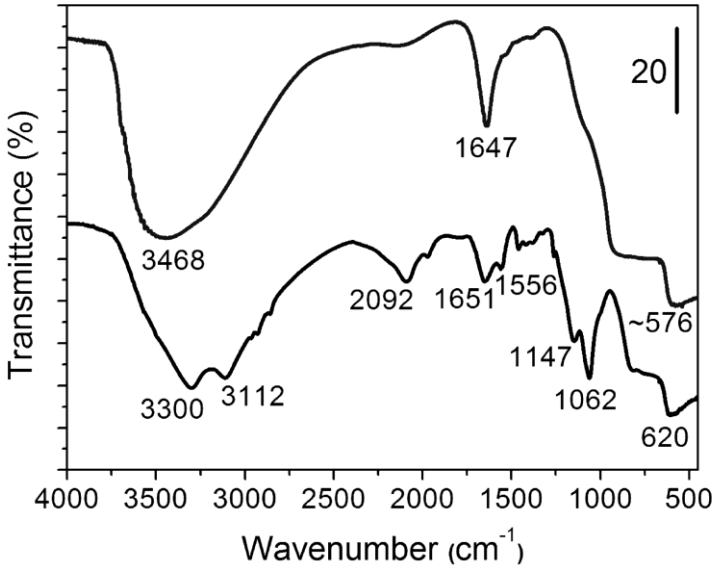
20
1647
3468
2092
1651
1556
~576
1147
1062
3300
3112
620
Transmittance (%)
4000
3500
3000
2500
2000
1500
1000
500
Wavenumber (cm-1)

Fig. 5

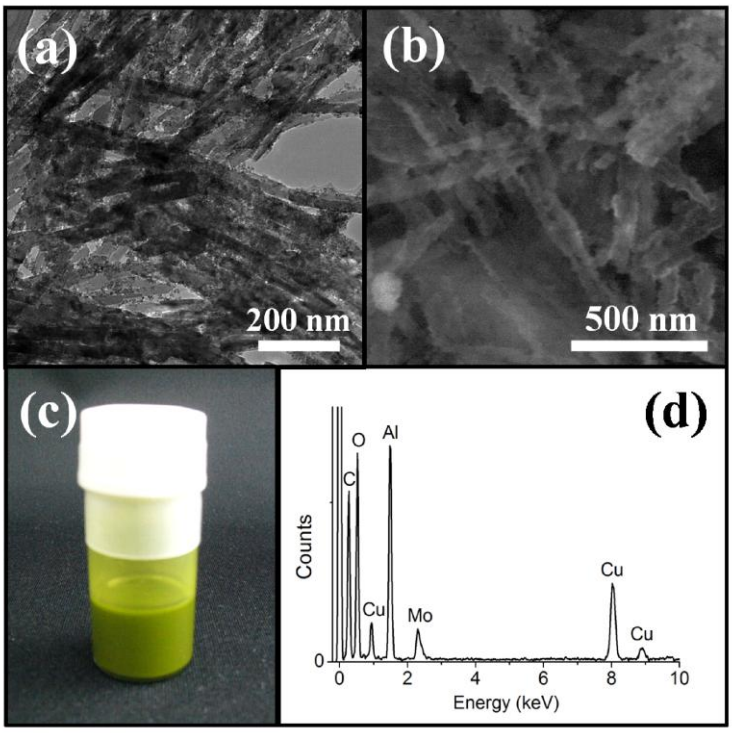

Fig. 6

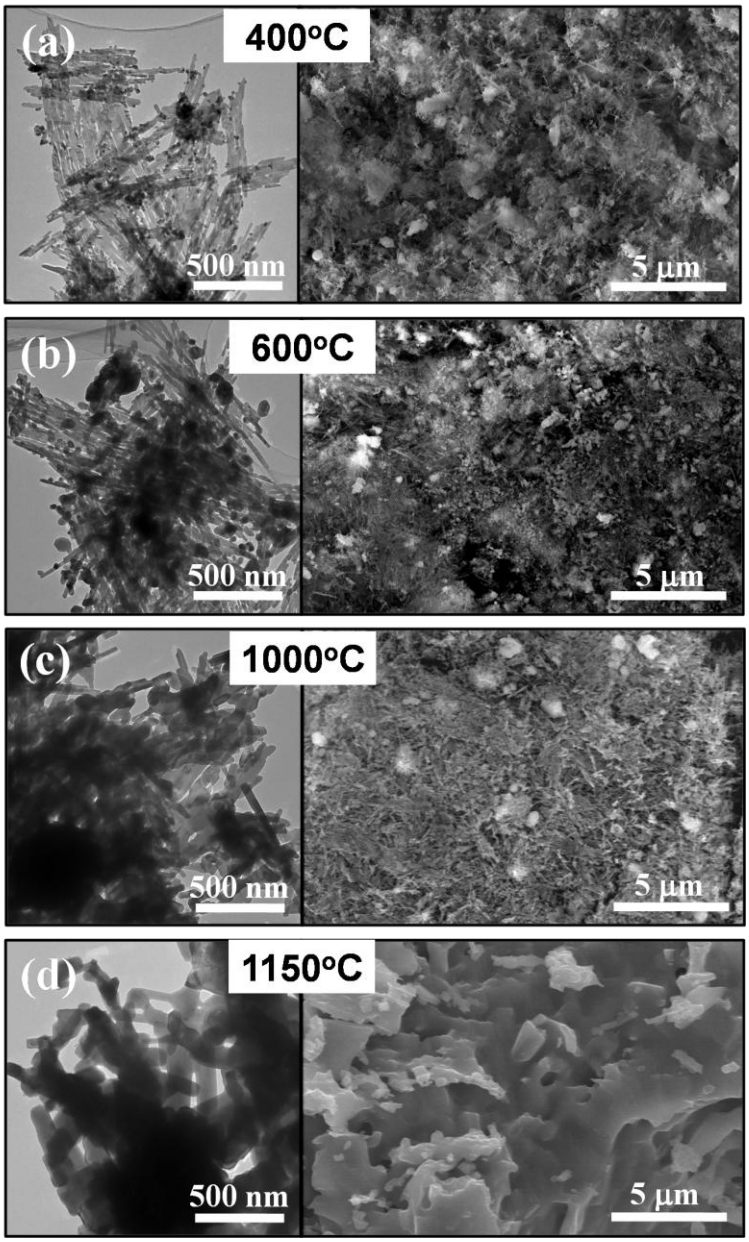
(a)
400°C
500 nm
5 µm
(b)
600°C
500 nm
5 µm
(c)
1000°C
500 nm
5 µm
(d)
1150°C
500 nm
5 µm

Fig. 7

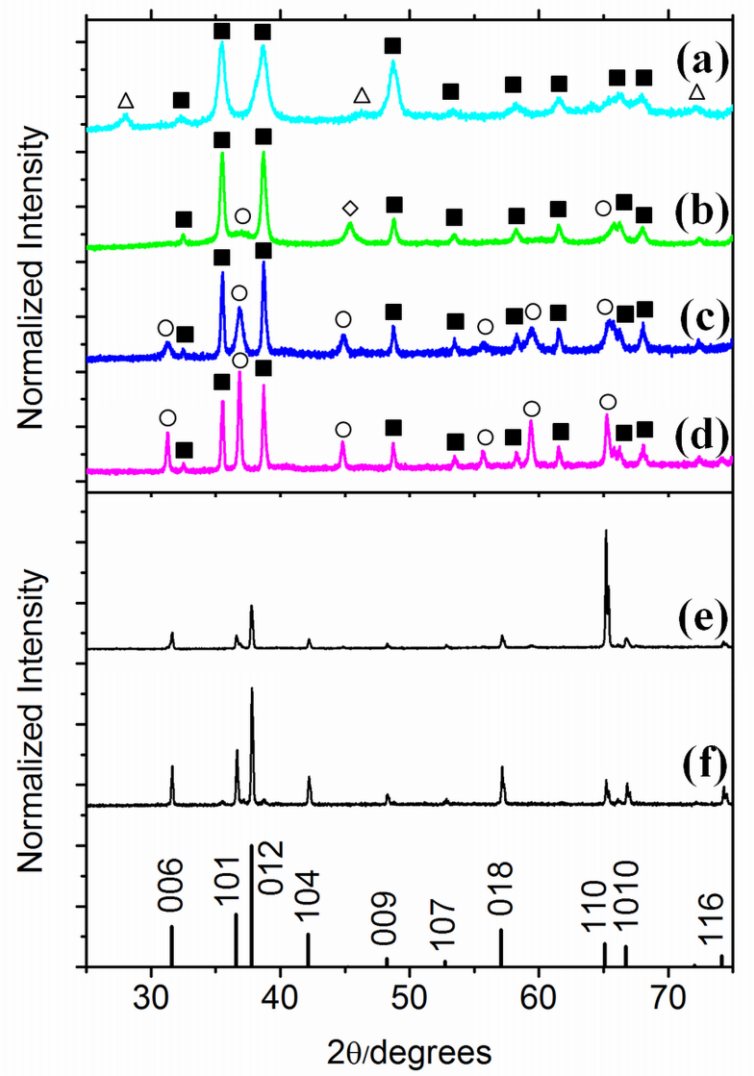
(a)
(b)
(c)
(d)
(e)
(f)
Normalized Intensity
Normalized Intensity
006
101
012
104
009
107
018
110
1010
116
30
40
50
60
70
2θ/degrees

Fig. 8

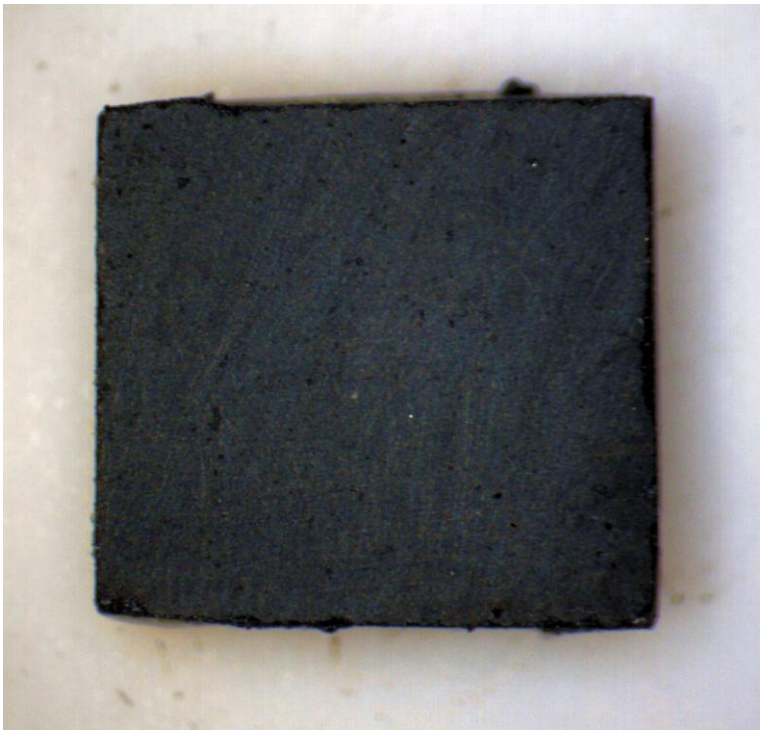

Fig. 9

*Graphical Abstract

Synthesis of Delafossite $CuAlO_2$ *p*-Type Semiconductor using a Nanoparticle-Based Cu(I) Acetate-Loaded Boehmite Precursor

T. V. Thu, P. D. Thanh, K. Suekuni, N. H. Hai, D. Mott, M. Koyano, and S. Maenosono

By annealing copper(I) acetate-loaded γ-AlOOH nanorods precursor at 1150 ºC, the (110)-oriented delafossite $CuAlO_2$ polycrystal was synthesized. The Seebeck measurement confirmed that the $CuAlO_2$ polycrystal has *p*-type conductivity with a relatively large Seebeck coefficient of 560 $\mu V \cdot K^{-1}$.

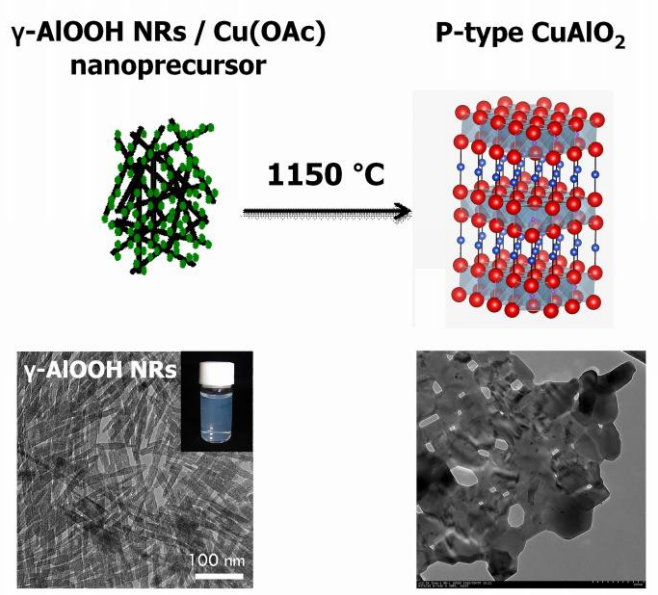

Highlights

> We developed a novel synthetic route for a delafossite $CuAlO_2$ *p*-type semiconductor. > Boehmite nanorods loaded with copper(I) acetate is used as a precursor. > The $CuAlO_2$ polycrystal exhibits the (110) orientation. > The Seebeck measurement for the $CuAlO_2$ polycrystal confirmed *p*-type conductivity.